Polymer Journal
https://doi.org/10.1038/s41428-024-00888-8

ORIGINAL ARTICLE

CO_2 gas-triggered wettability control of silylation-modified CNC films by manipulating the surface structure and introducing tertiary amino groups

Hiroyuki Taniyama[1,2] · Koji Takagi[2]

Received: 2 November 2023 / Revised: 17 December 2023 / Accepted: 18 December 2023

Abstract

Here, cellulose nanocrystal (CNC) films were chemically modified in a two-stage process to realize surface wettability control through the introduction of CO_2 gas. In addition to controlling the surface structure of the silylation-modified CNC film, functional groups derived from silane compounds were installed, and the corresponding effects on the resulting chemical modification were investigated. In the first stage, methyltriethoxysilane (MTES) and hexyltriethoxysilane (HTES) combined with tetraethoxysilane (TEOS) were subjected to condensation under alkaline conditions. In the second stage, (3-(*N*,*N*-dimethylamino)propyl)trimethoxysilane (DMAPS) generated an amino group to control the surface wettability by adsorption CO_2 gas. Then, the silylation-modified CNC film was fabricated on a glass substrate by spin coating. Fourier transform infrared (FT-IR), nuclear magnetic resonance (^{29}Si-NMR), and X-ray photoelectron spectroscopy (XPS) inspection indicated that the silane compounds were bonded to the CNC film surface and that tertiary amino groups were successfully introduced. The surface structure of the silylation-modified CNC film was analyzed by atomic force microscopy (AFM), and the surface roughness calculating indicated a root-mean-square roughness (RMS) of 4.2 nm. The water contact angles before and after the CO_2 gas treatment were evaluated as 73° and 22°, respectively.

Introduction

Toward realizing a circular economy, it is necessary to utilize naturally occurring raw materials. In particular, nanocellulose materials, such as cellulose nanofibers (CNFs) and cellulose nanocrystals (CNCs), have been intensively studied for their application as various functional materials [1–4]. The study of film functionalization using CNCs through a coating process has been conducted due to the favorable dispersion stability of sulfate salt-containing CNCs in water [5] and easy control of the viscosity of aqueous suspensions attributed to the moderate aspect ratio of CNCs [6, 7]. Functionalization using simple coating processes, such as spray coating, dip-coating, spin coating, and roller coating, is needed; these methods could be applied to various substrates and reduce energy consumption through the coating process. In particular, spin coating is a preferred process due to the controllability of the film thickness [8], minimization of required coating solution quantity, and ease of scaling up.

It has been reported that the film surface wettability could be controlled by chemical modification of CNCs [9–11]. The switchable wettability triggered by pH change, CO_2 adsorption, and UV radiation could be applied for various applications, such as oil-water separation, dye absorption, antifouling coatings, nanocomposites, bioengineering, droplet manipulation, and pattering [12]. In particular, the switchable wettability triggered by CO_2 gas is more sustainable than that triggered by other stimuli due to the lack of additional energy consumption [13]. For example, a mixture of polylactic acid (PLA) and a melamine derivative containing a tertiary amino group was cast on a glass substrate and then dried under a high humidity atmosphere. The obtained film has a honeycomb structure for

Supplementary information The online version contains supplementary material available at https://doi.org/10.1038/s41428-024-00888-8.

✉ Koji Takagi
takagi.koji@nitech.ac.jp

[1] Coating & Additives R&D Center, Coating & Additives Div. Mitsubishi Chemical Corporation, 1-2, Ushikawadori 4-chome, Toyohashi-shi, Aichi 440-8601, Japan

[2] Graduate School of Engineering, Nagoya Institute of Technology, Gokiso-cho, Showa-ku, Nagoya 466-8555, Japan

Published online: 15 February 2024

cell adhesion-controlled release for bioengineering applications [14]. The hydrophilicity and cell attachment properties of the obtained films were influenced by treatment with CO_2 gas. However, special knowledge and treatment for the drying process were required to create the honeycomb structure. As another example, after introducing a bromide-type initiator onto the surface of a poly(dopamine)-coated aluminum substrate, poly[2-(*N*,*N*-diethylamino)ethyl methacrylate] was grafted onto the film through surface-initiated atom transfer radical polymerization (SI-ATRP) [15]. Thus, the obtained coating film captured negatively charged silica gel particles in water after bubbling CO_2. Although the water contact angle could be controlled through CO_2 treatment, a tedious synthetic procedure should be considered for practical application. Therefore, preparing a chemically modified CNC film using a simple spin-coating method and controlling the surface wettability through treatment with CO_2 gas are effective techniques to create a smart functional surface.

We previously reported the phase separation of poly(-siloxane) during the silylation of CNCs in an aqueous solution and described the importance of the surface structure for attaining hydrophobic and hydrophilic surfaces [16]. The resulting nanosized beaded structure exhibited a large surface area and was useful for enhancing the surface hydrophobicity (hydrophilicity) and facilitating the introduction of functional groups. While amidine, guanidine, and imidazole are known to interact with CO_2 gas, considering the chemicals' ease of introduction and stability, we selected the tertiary amino group for further investigation [17]. Thus, silylation of CNCs was performed in a two-stage process using a set of silane compounds. A CNC film was fabricated via a spin-coating process, and the surface wettability was switched in water through the reaction of the tertiary amino group with CO_2 gas.

Experimental

Materials

CNCs (2.3–4.5 nm in diameter, 44–108 nm in length, and 0.8% sulfur) were purchased from CelluForce, Inc. Hexyltriethoxysilane (HTES), methyltriethoxysilane (MTES), tetraethoxysilane (TEOS), 3-(*N*,*N*-dimethylamino)propyl) trimethoxysilane (DMAPS), ethanol, and aqueous ammonia (NH_3) solution (25%) were purchased from Sigma–Aldrich, Japan, K. K. All chemicals were used as received.

Sample Preparation of the CNC/TEOS/HTES suspension

CNCs (1.0 g) were added to deionized water (70 g), and a suspension was obtained after sonication at 20 kHz and 30% power using an ultrasonic homogenizer (Yamato Scientific Co., Ltd., LUH300) for 3 min at room temperature. Ethanol (130 g), HTES (0.24 g), TEOS (0.26 g), and NH_3 solution (0.17 g) were added to the CNC suspension. The mixture was stirred at 300 rpm for 60 min at room temperature and then held at room temperature for 1 day.

Sample preparation of the CNC/TEOS/HTES/DMAPS suspension

DMAPS (0.46 g) was added to the aforementioned CNC/TEOS/HTES suspension. The mixture was stirred at 300 rpm for 120 min at room temperature.

Coating process

The suspension (2 mL) was placed on a glass substrate (15 cm square), accelerated at 40 rpm/s, and spun at 400 rpm for 60 s. Thereafter, the coated glass substrate was placed in a heat oven at 100 °C for 2 h to dry and facilitate condensation.

Surface wettability switching test triggered by CO_2 gas

The coating sample was immersed in water, CO_2 gas was bubbled through at a rate of 10 L/min for 1 min, and then the sample was continuously immersed in CO_2-bubbled water at room temperature for 1 h. Subsequently, the water droplets on the surface were removed though an air spray. Water contact angle measurements were subsequently conducted to obtain the dried samples.

Characterization

Fourier transform infrared (FT-IR) spectra (Thermo Scientific Nicolet iS5, Ge-ATR) were collected in the spectral range of 400–4000 cm^{-1} with 32 scans and a resolution of 4 cm^{-1}. X-ray photoelectron spectroscopy (XPS) was performed using a K-α spectrometer (XPS Thermo K-alpha). The region of analysis was 400 mm Φ. Wide scans were conducted with a 200 eV pass energy and a 1.0 eV step size. High-resolution scans were conducted with a 50 eV pass energy and a 0.1 eV step size. The obtained binding energy was calibrated by the C 1 s peak at 284.8 eV. ^{29}Si nuclear magnetic resonance (NMR) spectra were recorded with a JNM-ECA600II (JEOL). Atomic force microscopy (AFM) was performed in tapping mode using a Hitachi high-tech instrument (SPI4000) and standard tapping mode probes. The water contact angle of the CNC-coated glass substrate was measured using a Drop Master 500 (Kyowa Chemical Industry Co.). The volume of the dropped liquid was 10 μL, and the contact angle was recorded after 2 s after contact with the surface.

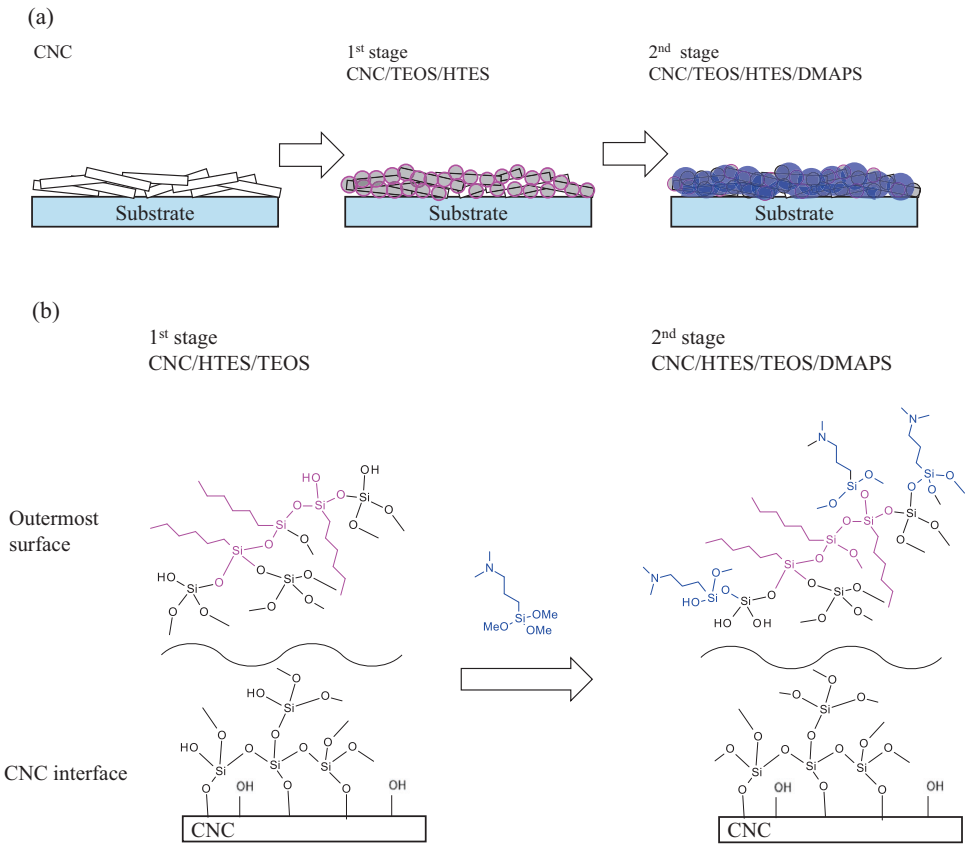

Fig. 1 **a** Schematic illustration of the silylation modification of CNC by using TEOS, HTES, and DMAPS in two-stage process. **b** Proposed chemical composition at each interface

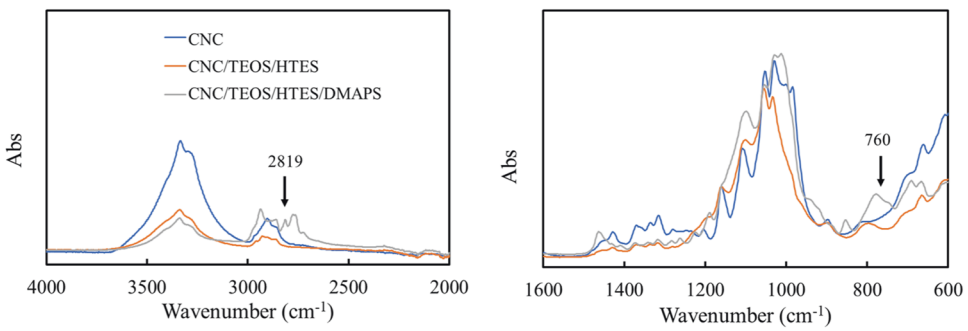

Fig. 2 FT-IR spectra of CNC, CNC/TEOS/HTES, and CNC/TEOS/HTES/DMAPS (ATR method)

Results and discussion

To control the surface wettability of a CNC film triggered by CO_2 gas, a two-stage silylation modification method was applied. In the first stage, a nanosized surface structure was formed on the CNCs by using MTES and TEOS as coprecursors, as described in our previous study [16]. In the second stage, to introduce the tertiary amino group and switch the wettability by CO_2, DMAPS was condensed with the silylation-modified CNCs obtained in the first stage. In the first stage, the quantity of the unreacted silanol-type hydroxy group was adjusted by controlling the MTES/TEOS ratio. Specifically, we changed the MTES/TEOS molar ratio to 0.8, which is nearly half the value used in our previous study (1.5) [16]. Furthermore, the alkyl chain was changed from a methyl group to a hexyl group to enhance the wettability before and after CO_2 treatment. A schematic illustration of these processes and the chemical composition at each interface is shown in Fig. 1. To confirm the chemical composition of the silylation-modified CNCs, the FT-IR spectrum of each sample (for which the thickness of the casted film was approximately 10 μm) was analyzed (Fig. 2). The obtained spectra were normalized by the peak at 1160 cm^{-1} attributed to asymmetric glycoside vibration [18]. The peak attributed to the stretching vibration of Si-O-C at 762 cm^{-1} was observed, indicating interfacial bonding between the hydroxyl groups of CNCs and the silanol groups of the silane compounds [19]. The reduced peak intensity could be correlated with both the amount of silane compound introduced as a modifier and the reaction

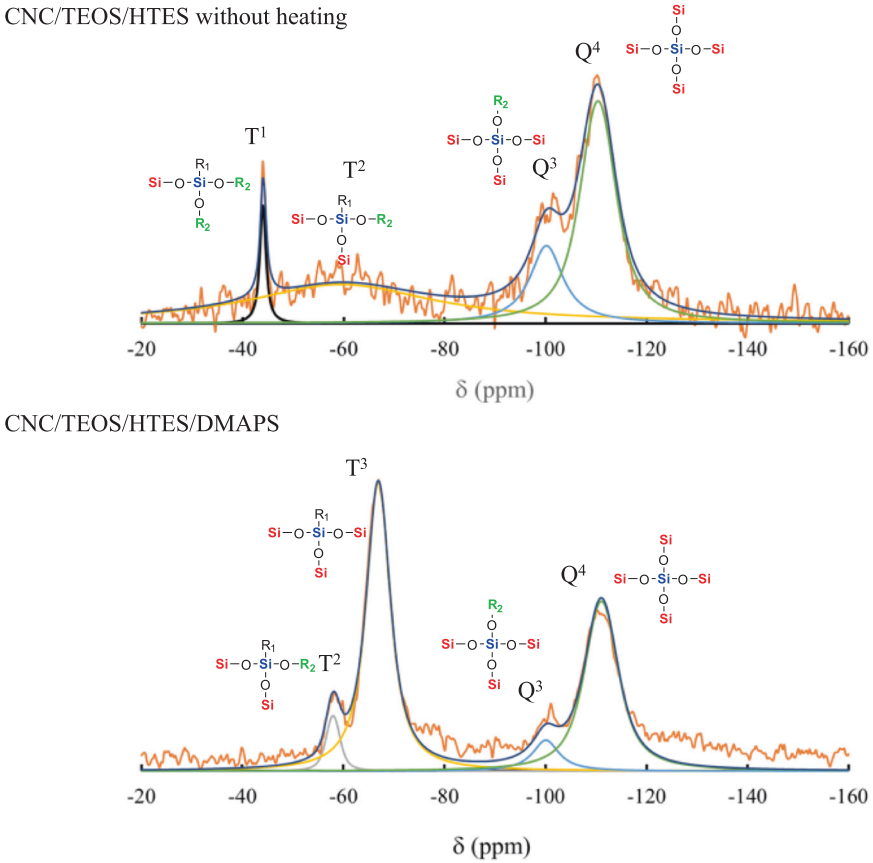

Fig. 3 Solid-state ^{29}Si NMR spectra of the silylation-modified CNC

conditions of the silylation modification. In this case, the weight ratio of total silane compounds to CNCs was 0.5 in the first stage when using TEOS/HTES and 1.0 in the second stage when using TEOS/HTES/DMAPS. Two factors should be considered when determining the feed ratio of silica precursors to CNCs. First, to completely cover the CNC surface, a sufficient amount of silane compounds must be added. Second, if an excessive amount of silane compounds is added, the influence of the treatment on the resulting CNCs will not be fully elucidated. When the sol–gel reaction was performed in the presence of CNCs, the surface roughness and water contact angle actually changed (*vide infra*). Although the thickness of the CNC/silica hybrid film was not measured and the feed ratio of silica precursor to CNC was not optimized in the present system, indicating that CNCs play an important role in forming the surface structure on the glass substrate. Under acidic conditions, the hydrolysis and condensation of silane compounds tend to form a linear chain structure [20]. Therefore, we performed silylation under alkaline conditions to obtain a rough film surface structure. These reaction conditions yielded three-dimensional growth of the siloxane network on the CNC surface and a decrease in the relative Si-O-C peak intensity (see also Fig. 1b). After the introduction of DMAPS, the peak at 2819 cm^{-1} related to the asymmetric stretching vibration of N-C-H [21] was confirmed, which qualitatively supported the successful introduction of tertiary amino groups.

To confirm the siloxane network structures and monitor the reaction progress during condensation of the silane compounds, solid-state ^{29}Si NMR spectra were collected (Fig. 3). When DMAPS was reacted in the second stage, the molar ratio of TEOS/HTES/DMAPS became 28/22/50, and the excess amount of DMAPS was used to impart the wettability change property triggered by the CO_2 gas. In the case of CNC/TEOS/HTES, to facilitate the introduction of DMAPS on the surface, heat treatment was not applied. The T^1 (9%) and T^2 (91%) peaks derived from HTES and the Q^3 (26%) peak derived from TEOS were observed, which indicated that the silylation-modified CNCs prepared by using TEOS/HTES as coprecursors in the first stage have enough potential to introduce DMAPS in the second stage. After introducing DMAPS to CNC/TEOS/HTES and heating at 100 °C for 2 hr, the condensation reaction of TEOS, HTES, and DMAPS progressed, resulting in an increase in the ratio of Q^4 from 74 to 87%, and the integral ratio of the T^3 peak (91%) was greater than that of the T^2 peak (9%).

To evaluate the chemical composition of the CNCs and silylation-modified CNCs, XPS was performed, and the peak intensities of the CNCs, CNCs/TEOS/HTES, and

CNCs/TEOS/HTES/DMAPS were plotted as a function of the binding energy (Fig. 4). For the unmodified CNCs, peaks at 286.6 eV corresponding to the carbon atom (C 1 s) and 531.5 eV corresponding to the oxygen atom (O 1 s) were observed. For CNC/TEOS/HTES, new silicon atom-derived peaks appeared at 103.6 eV and 153.1 eV corresponding to Si 2p and Si 2 s, respectively. After the condensation of DMAPS in the second stage, a new peak appeared at 400.0 eV corresponding to the nitrogen atom (N 1 s), which indicated that the tertiary amino group was introduced, which agreed with the results of the FT-IR analyses. Considering the broader C 1 s peak, we performed peak deconvolution for the silylation-modified CNC film in both the first stage and second stage to determine the introduction of functional groups [18, 22]. For the unmodified CNCs, peak deconvolution indicated that the C 1 s peak mainly consisted of the C-O peak at 286.5 eV (Table S2). After introducing TEOS and HTES in the first stage, the peak corresponding to the C-C/C-Si group at 284.8 eV evolved, and the atomic concentration in the lower energy region increased. Unfortunately, after introducing DMAPS in the second stage, no noticeable change in the relative intensity of the peaks was observed, likely due to the overlap of the C-N and C-Si peaks. In comparison to the CNC/TEOS/HTES/DMAPS system, the CNC/TEOS/MTES/DMAPS system in which the methyl group was introduced instead of the hexyl group was also evaluated via XPS (Fig. S1). The C 1 s/Si 2p ratio related to the amount of carbon chain per silicon element was calculated as 2.0 for the MTES system and 4.9 for the HTES system, which likely indicates that the alkyl chain in the HTES system could influence the surface properties more than the alkyl chain in the MTES system (Table S3). Furthermore, the simultaneous addition of TEOS, HTES, and DMAPS to the CNC suspension was also investigated. The N component derived from the tertiary amino group was clearly reduced compared to that in the two-stage process (Table S3), which indicates that the tertiary amino groups were efficiently localized on the outermost surface in the two-stage modification process.

To gain insight into the CNC surface structure formed by the silylation modification, AFM was performed. The CNC film had a rod-like surface structure (Fig. 5a), while the silylation-modified CNC film obtained using TEOS/HTES in the first stage had a beaded structure along with the CNC rod (Fig. 5b). Like in our previous research, the hydrophobic interaction of the hexyl group in HTES progressed in a polar water/ethanol mixed solvent, resulting in phase separation. Moreover, a beaded structure was maintained, and the particle size increased after modification with DMAPS in the second stage (Fig. 5c), indicating that DMAPS covers the surface of CNC/TEOS/HTES. The change in the particle size is consistent with the weight ratio

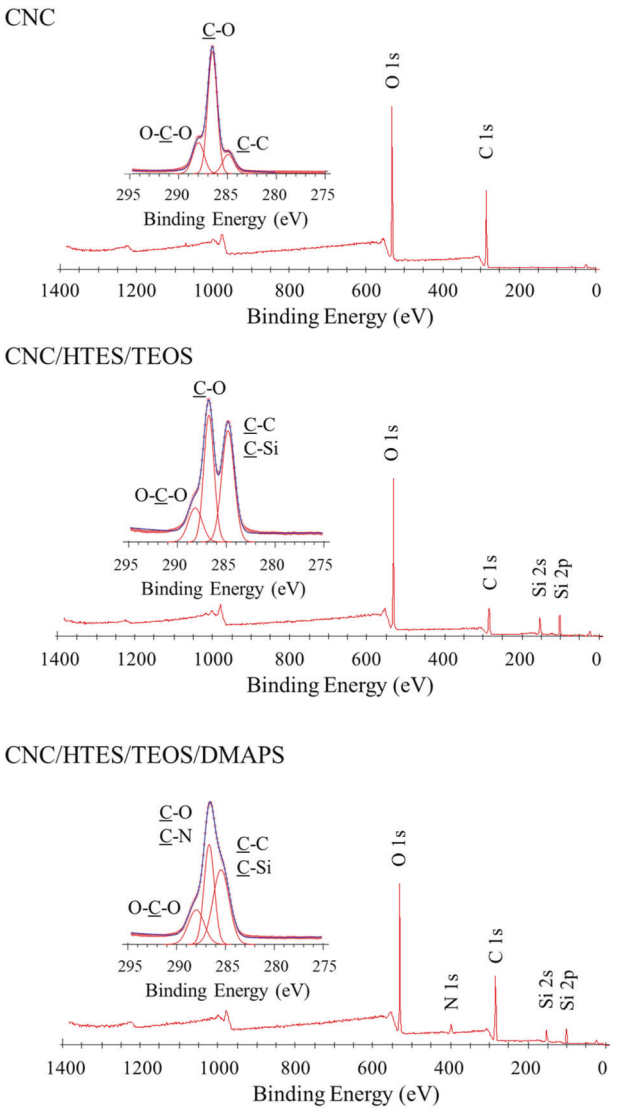

Fig. 4 XPS survey spectra of the CNC, CNC/TEOS/HTES, and CNC/TEOS/HTES/DMAPS. Inset shows the high-resolution analysis of C 1 s peak with a peak deconvolution

of the added silane compounds, namely, Si/CNC = 0.5 in the first stage and Si/CNC = 1.0 in the second stage. When MTES was used instead of HTES, a similar beaded structure with a comparable particle size was formed before and after modification with DMAPS (Fig. 5d, e). The rod length of the CNCs was 91 nm (Fig. 5a), and the sizes of the silica particles in the CNC/TEOS/HTES and CNC/TEOS/HTES/DMAPS samples were calculated to be 31 nm (Fig. 5b) and 66 nm (Fig. 5b), respectively, from the AFM image and ImageJ software analysis. Figure 5a, b, d, which were obtained without DMAPS functionalization, show anisotropy due to the centrifugal force generated during spin coating. As shown in Fig. 5c, e, after DMAPS functionalization, the beaded structure was not anisotropic. In contrast to the two-stage modification process that results in a

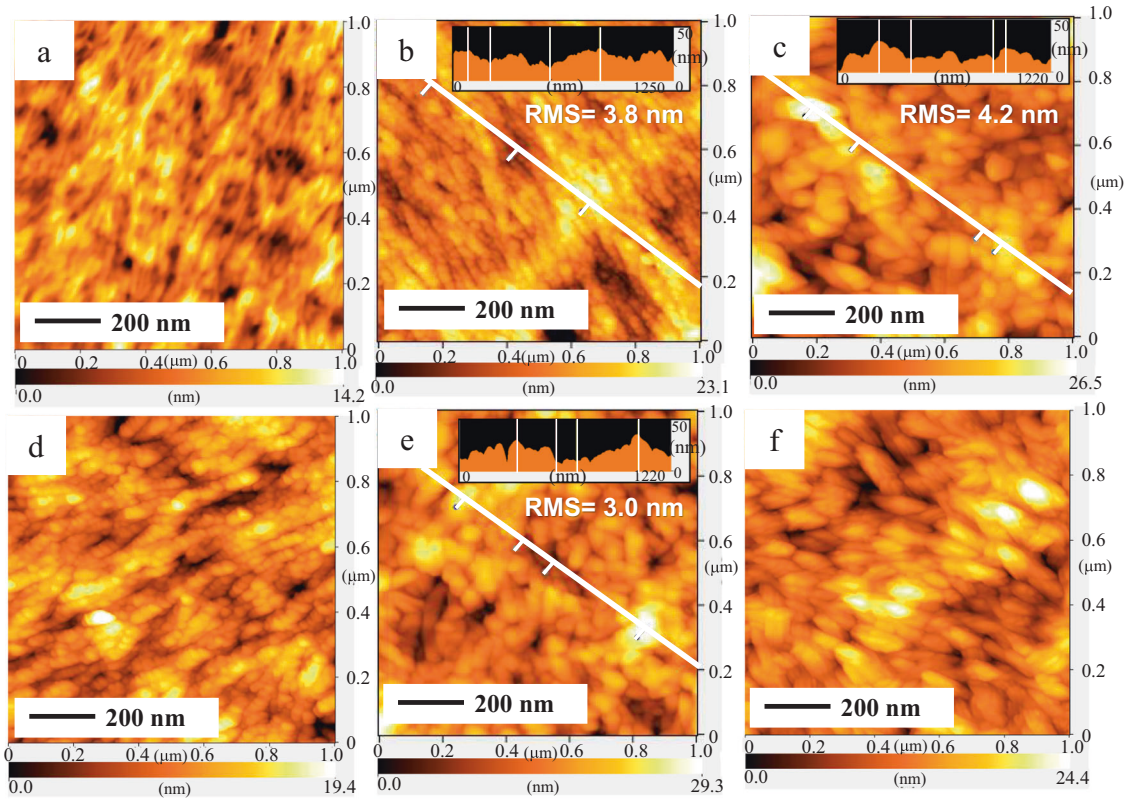

Fig. 5 AFM images of (**a**) CNC, (**b**) CNC/TEOS/HTES, (**c**) CNC/TEOS/HTES/DMAPS, (**d**) CNC/TEOS/MTES, (**e**) CNC/TEOS/MTES/DMAPS, and (**f**) CNC/TEOS/HTES/DMAPS, where only (**f**) was obtained by the simultaneous modification method

Table 1 Water contact angles and surface roughness of each sample

Silane compounds for CNC modification	Process	WCA (°)			RMS roughness (nm)
		before CO_2 treatment	after CO_2 treatment	after H_2O treatment	
Unmodified CNC	–	28	–	–	2.4
TEOS/HTES	First stage	83	81	83	3.8
TEOS/HTES/DMAPS	Second stage	73	22	67	4.2
TEOS/MTES/DMAPS	Second stage	62	38	–	3.0
TEOS/HTES/DMAPS	Simultaneous	70	63	–	3.9

beaded structure, the simultaneous addition of TEOS, HTES, and DMAPS into an aqueous suspension of CNCs resulted in a spheroid structure, as indicated in Fig. 5f. The structural difference due to the modification process is attributed to the polarity of the functional groups of the silane compounds [23]. In the simultaneous modification method, the coexistence of the hexyl groups of HTES and the tertiary amino groups of DMAPS likely influenced the hydrophobic interaction of alkyl chains during the phase separation step, although further investigation is still needed. The surface morphology and surface roughness (root-mean-square roughness RMS) were quantitatively investigated via AFM. The RMS of the unmodified CNCs was 2.4 nm, whereas that of the CNCs/TEOS/HTES obtained in the first-stage modification was 3.8 nm (Table 1). After the second-stage modification, the RMS value of CNC/TEOS/HTES/DAMPS became 4.2 nm, which was greater than the value in the first stage, probably due to the increase in the particle size. The RMS value was 3.9 nm in the simultaneous modification system, and no significant difference was observed because the Si/CNC weight ratio was the same.

To evaluate the surface wettability of the silylation-modified CNCs, water contact angle measurements were conducted for the spin-coated films (Table 1). The contact angle of the CNC/TEOS/HTES film was 83°, which increased from that of the CNC film (28°) due to the introduction of hydrophobic hexyl chains. However, after

modification with DMAPS, the contact angle decreased (73°), indicating that the polarity of the silylation-modified CNC film surface increased due to the presence of the tertiary amino group. Subsequently, changes in surface wettability were investigated by bubbling CO_2 gas through the water in which the CNC/TEOS/HTES and CNC/TEOS/HTES/DMAPS films were immersed. The water contact angle of the CNC/TEOS/HTES film after CO_2 treatment was 81°, which was the initial value and indicated that there was no CO_2 response. However, in the case of the CNC/TEOS/HTES/DMAPS film, the water contact angle decreased after CO_2 treatment (22°) [24]. This result is attributed to CO_2 adsorption on tertiary amino groups, and the formation of an ammonium bicarbonate structure is responsible for these changes in wettability [25, 26]. To confirm the formation of ammonium bicarbonate, CNCs were modified with only DMAPS for CO_2 adsorption experiments. After CO_2-bubbled water immersion treatment, the peak at 1645 cm^{-1} related to the asymmetric COO^- vibration of bicarbonate anions was confirmed, which qualitatively supported the successful formation of ammonium bicarbonate (Fig. S2). However, in the CNC/TEOS/HTES/DMAPS system, the corresponding signal could not be clearly confirmed, probably due to the small number density of the tert-amino groups. Namely, the number density of the tert-amino groups in the spin-coated film was calculated to be 1.2 $mmol_N/g$ based on the film thickness (175 nm) and feed ratio of each silane compound. The obtained value was small compared to the value (2.1 $mmol_N/g$) obtained when DMAPS was functionalized on the surface of porous SBA-15 [25]. However, based on the literature and our preliminary experiments, we believe that ammonium bicarbonate was formed. As shown by the AFM morphology of the CNCs/TEOS/HTES/DMAPS after CO_2 treatment, the surface morphology and roughness (4.2 nm) did not change drastically (Figure not shown). Because we could not collect experimental evidence to completely exclude the formation of amorphous organosilica particles, we performed an additional sol-gel reaction without CNCs using TEOS/HTES (first stage) and DMAPS (second stage) for reference. If the film surface was mainly covered by amorphous organosilica particles, then the surface roughness and water contact angle should be comparable. As a result, the surface roughness of the spin-coated film without CNCs was determined to be RMS = 2.9 nm based on the AFM measurements (Fig. S3), and the water contact angles were 63° and 38° before and after the CO_2 gas treatment, respectively. These results showed that CNCs improved the surface roughness of the film and enhanced the surface wettability, as we expected (see Fig. 1a). As a comparison of the surface wettability switching triggered by CO_2, the water contact angle was also measured after immersing the silylation-modified CNC film in water without CO_2 bubbling. The water contact angles of the CNC/TEOS/HTES film and CNC/TEOS/HTES/DMAPS film were 83° and 67°, respectively, which nearly maintained the initial values. These results showed that the change in the water contact angle was caused by the CO_2 treatment. We compared the wettability switching performance of film surfaces with that of CO_2 to that of a previous study reported by Yin and coworkers [14]. A previous study reported that the water contact angle was changed from 98° to 63° through CO_2 treatment. Focusing on the change in the water contact angle, in the present study, high contrast values were achieved through CO_2 treatment by controlling the nanostructure of the CNC-applied film surface using a two-stage modification approach. It was reported that CO_2 was desorbed through N_2 bubbling, and the water contact angle returned to the initial value in a previous study [14]. We also conducted a similar experiment; however, the water contact angle of the CNC/TEOS/HTES/DMAPS film did not return to the initial value after N_2 bubbling treatment (the water contact angles before and after N_2 bubbling treatment were 22° and 39°, respectively). Although we have not yet reached a conclusion on this point, we consider that the surface structure of the film may influence these results. In a previous study, the size of the voids that formed on the film surface was several micrometers, whereas in this study, this value was several tens of nanometers based on the AFM observation results. Therefore, CO_2 was not considered to be sufficiently desorbed by the N_2 bubbling treatment due to the mismatch in size between the film roughness and N_2 bubbles. Similarly, the wettability change triggered by CO_2 gas was investigated for the MTES system. The water contact angle was 62° after introducing DMAPS. The smaller water contact angle compared with that of the CNC/TEOS/HTES/DMAPS system is likely ascribed to the shorter methyl chain [27] as well as the smaller surface roughness of the silylation-modified CNC film (RMS = 3.0 nm) compared with that of the HTES system (RMS = 3.8 nm). Because the water contact angle after CO_2 treatment of the MTES system was 38°, the introduction of a hexyl group is useful for achieving a large change in the surface wettability triggered by CO_2. The water contact angle of the CNC/TEOS/HTES/DMAPS film obtained via the simultaneous modification method was also investigated. The water contact angle after CO_2 bubbling treatment was 63°, which was greater than that of the two-stage modification system (22°). This result can be explained by the fact that the amount of tertiary amino groups on the silylation-modified CNC film surface was lower in the simultaneous modification system than in the two-stage modification system, as discussed in the XPS analysis section. Hence, these results showed that the adoption of the two-stage modification process enhanced the surface wettability switching function triggered by CO_2

gas. Importantly, CNCs not only serve as anchors for binding functional groups but also serve to create nanosized rough structures on substrates to enhance surface functionality.

Conclusions

In this study, the wettability change triggered by CO_2 gas was achieved by controlling the surface structure of silylation-modified CNC films using HTES and TEOS as coprecursors and introducing DMAPS containing tertiary amino groups. The chemical composition of the silylation-modified CNC film was evaluated by FT-IR, ^{29}Si-NMR, and XPS. The water contact angles before and after the CO_2 treatment were evaluated. As a result, the wettability could be controlled by CO_2 adsorption, and the introduction of hexyl and tertiary amino groups in the two-stage process is shown to be quite important for realizing significant changes in the water contact angle. These results indicate that the silylation-modified CNCs can be applied in various applications, such as protective coating and oil-water separation.

Funding Open Access funding provided by Nagoya Institute of Technology.

Compliance with ethical standards

Conflict of interest The authors declare no competing interests.

Publisher's note Springer Nature remains neutral with regard to jurisdictional claims in published maps and institutional affiliations.

References

1. Zhu Z, Fu S, Lavoine N, Lucia LA. Structural reconstruction strategies for the design of cellulose nanomaterials and aligned wood cellulose-based functional materials – a review. Carbohydr Polym. 2020;247:116722.
2. Calvino C, Macke N, Kato R, Rowan SJ. Development, processing and applications of bio-sourcedcellulose nanocrystal composites. Prog Polym Sci. 2020;103:101221.
3. Sharma A, Thakur M, Bhattacharya M, Mandal T, Goswami S. Cellulose nanocrystal based multifunctional nanohybrids. Prog Mater Sci. 2020;112:100668.
4. Gomri C, Cretin M, Semsarilar M. Recent progress on chemical modification of cellulose nanocrystal (CNC) and its application in nanocomposite films and membranes-a comprehensive review. Carbohydr Polym. 2022;294:119790.
5. Ranjbar D, Hatzikiriakos SG. Effect of ionic surfactants on the viscoelastic properties of chiralnematic cellulose nanocrystal suspensions. Langmuir. 2020;36:293.
6. Ching YC, Ali ME, Abdullah LC, Choo KW, Kuan YC, Julaihi SJ, et al. Rheological properties of cellulose nanocrystal-embedded polymer composites: a review. Cellulose. 2016;23:1011.
7. Kar H, Sun J, Clewett CFM, Thongsai N, Paoprasert P, Dwyer JH, et al. Uniform amphiphilic cellulose nanocrystal films. Polym J. 2022;54:539–50.
8. Higaki Y, Takahara A. Structure and properties of polysaccharide/imogolite hybrids. Polym J. 2022;54:473–9.
9. Huang X, Wang A, Xu X, Liu H, Shang S. Enhancement of hydrophobic properties of cellulose fibers via grafting with polymeric epoxidized soybean oil. ACS Sustain Chem Eng. 2017;5:1619.
10. Yuan Z, Wen Y. Enhancement of hydrophobicity of nanofibrillated cellulose through grafting of alkyl ketene dimer. Cellulose. 2018;25:6863.
11. Le D, Kongparakul S, Samart C, Phanthong P, Karnjanakom S, Abudula A, et al. Preparing hydrophobic nanocellulose-silica film by a facile one-pot method. Carbohydr Polym. 2016;153:266.
12. Liu H, Zhang L, Huang J, Mao J, Chen Z, Mao Q, et al. Smart surfaces with reversibly switchable wettability: concepts, synthesis and applications. Adv Colloid Interface Sci. 2022;300:102584.
13. Li Y, Zhu L, Grishkewich N, Tam KC, Yuan J, Mao Z, et al. CO_2-responsive cellulose nanofibers aerogels for switchable oil—water separation. ACS Appl Mater Interfaces. 2019;11:9367.
14. Yin H, Zhan F, Li Z, Huang H, Marcasuzaa P, Luo X, et al. CO_2-triggered on/off wettability switching on bioinspired polylactic acid porous films for controllable bioadhesion. Biomacromolecules. 2021;22:1721–9.
15. Liu H, Yuan X, Ho J, Cunningham MF, Oleschuk RD, Jessop PG. A CO_2-switchable surface on aluminium. Appl Surf Sci. 2020;525:146630.
16. Taniyama H, Takagi K. Study on controlling the surface structure and properties of a cellulose nanocrystal film modified using alkoxysilanes in green solvents. Langmuir. 2022;38:5550.
17. Liu H, Lin S, Feng Y, Theato P. CO_2-responsive polymer materials. Polym Chem. 2017;8:12.
18. Cabrera IC, Berlioz S, Fahs A, Louarn G, Carriere P. Chemical functionalization of nano fibrillated cellulose by glycidyl silane coupling agents: a grafted silane network characterization study. Int J Biol Macromol. 2020;165:1773–82.
19. Dhali K, Daver F, Gass P, Adhikari B. Surface modification of the cellulose nanocrystals through vinyl silane grafting. Int J Biol Macromol. 2022;200:397.
20. Cai S, Zhang Y, Zhang H, Yan H, Lv H, Jiang B. Sol—gel preparation of hydrophobic silica antireflective coatings with low refractive index by base/acid two-step catalysis. ACS Appl Mater Interfaces. 2014;6:11470.
21. Eskandari P, Rezvani ZA, Mamaqani HR, Kalajahi MS. Carbon dioxide-switched removal of nitrate ions from water by cellulose nanocrystal-grafted and free multi-responsive block copolymers. Mol J Liq. 2020;318:114308.

22. Qu M, Pang Y, Li J, Wang R, He D, Luo Z, et al. Eco-friendly superwettable functionalized-fabric with pH-bidirectional responsiveness for controllable oil-water and multi-organic components separation. Colloids Surf A Physicochem Eng Asp. 2021;624:126817.
23. Taniyama H, Takagi K. Controlling the surface structure and functionalization of a cellulose nanocrystal film modified by using glycidyloxypropylsilane in a coating process. Polym J. 2023;55:675.
24. We also measured the water contact angle of the sample that was dried in a vacuum oven after CO_2-bubbled water immersion treatment. *The water contact angle showed the same vale (22°) regardless of the vacuum drying operation implying that the air spray drying is sufficient for the experiment*.
25. Lee JJ, Chen CH, Shimon D, Hayes SE, Sievers C, Jones CW. Effect of humidity on the CO_2 adsorption of tertiary amine grafted SBA-15. J Phys Chem C. 2017;121:23480.
26. Foo GS, Lee JJ, Chen CH, Hayes SE, Sievers C, Jones CW. Elucidation of surface species through in situ FTIR spectroscopy of carbon dioxide adsorption on amine-grafted SBA-15. Chem Sus Chem. 2017;10:266.
27. Berrera EG, Livotto PR, dos Santos JHZ. Hybrid silica bearing different organosilanes produced by the modified Stöber method. Powder Technol. 2016;301:486.